Complex antiferromagnetic order in the garnet $Co_3Al_2Si_3O_{12}$

Q. Cui,[1,7] Q. Huang,[2] Jose A. Alonso,[3] Denis Sheptyakov,[4] C. R. De la Cruz,[5] M. T. Fernández-Díaz,[6] N. N. Wang,[1,7] Y. Q. Cai,[1] D. Li,[1,7] X. L. Dong,[1,7,8] H. D. Zhou,[2] and J.-G. Cheng[1,7,8,*]

[1]*Beijing National Laboratory for Condensed Matter Physics and Institute of Physics, Chinese Academy of Sciences, Beijing 100190, China*
[2]*Department of Physics and Astronomy, University of Tennessee, Knoxville, Tennessee 37996, USA*
[3]*Instituto de Ciencia de Materiales de Madrid, CSIC, Cantoblanco, E-28049 Madrid, Spain*
[4]*Laboratory for Neutron Scattering and Imaging, Paul Scherrer Institut, 5232 Villigen PSI, Switzerland*
[5]*Quantum Condensed Matter Division, Oak Ridge National Laboratory, Oak Ridge, Tennessee 37381, USA*
[6]*Institut Laue Langevin, BP 156X, Grenoble F-38042, France*
[7]*School of Physical Sciences, University of Chinese Academy of Sciences, Beijing 100190, China*
[8]*Songshan Lake Materials Laboratory, Dongguan, Guangdong 523808, China*

(Received 10 January 2020; revised manuscript received 21 March 2020; accepted 31 March 2020; published 20 April 2020)

We studied the magnetic properties of the garnet $Co_3Al_2Si_3O_{12}$ synthesized under 5.5 GPa and 1250 °C by means of dc magnetic susceptibility, neutron powder diffraction, and specific heat. Although the magnetic Co^{2+} ions form a geometrically frustrated hyper-Kagome lattice, we find that $Co_3Al_2Si_3O_{12}$ exhibits a long-range antiferromagnetic order below $T_N = 11$ K without showing magnetic frustration, i.e., the frustration index $f \equiv |\theta_{CW}/T_N|$ is close to unity. Refinements from neutron-diffraction data show that $Co_3Al_2Si_3O_{12}$ forms a complex antiferromagnetic structure characterized by the coexistence of collinear and commensurate spiral magnetic ordering of Co^{2+} sublattices. Magnetic field induced spin-flop transition at $\mu_0 H_c \approx 4$T was also observed below T_N.

DOI: 10.1103/PhysRevB.101.144424

I. INTRODUCTION

Magnetic materials based on the triangular structural unit are usually prone to geometrical frustration, which is at the origin of many unconventional magnetic phenomena [1]. The quasi-two-dimensional (q2D) antiferromagnets with triangular or Kagome lattices are of particular interest and have been extensively explored in the past decades. For example, the long-sought quantum spin-liquid state has been arguably realized in q2D triangular lattice antiferromagnets (TLAFs) $YbMgGaO_4$ [2–4], $NaYbS_2$ [5], 6HB-$Ba_3NiSb_2O_9$ (high-pressure phase) [6,7], and the herbertsmithite $ZnCu_3(OH)_6Cl_2$ with Kagome lattice [8,9]. Even for the TLAFs with conventional 120° spin structure, an unusual up-up-down (uud) state manifested by a magnetization plateau at $1/3M_s$ over a finite magnetic field range has been theoretically predicted for various spin numbers by considering either quantum or thermal fluctuations [10–12]. Experimentally, such a uud state has been observed in several TLAFs, including Cs_2CuBr_4 with S-1/2 Cu^{2+} magnetic ions [13,14], $Ba_3CoSb_2O_9$ and $Ba_3CoNb_2O_9$ with effective S-1/2 Co^{2+} ions [15–17], $Ba_3NiSb_2O_9$ (ambient-pressure phase) and $Ba_3NiNb_2O_9$ with S-1 Ni^{2+} ions [18,19], $RbFe(MoO_4)_2$ with S-5/2 Fe^{3+} ions [20,21], $Rb_4Mn(MoO_4)_3$ and $Ba_3MnNb_2O_9$ with S-5/2Mn^{2+} ions [22,23], etc.

In contrast to many q2D TLAFs mentioned above, the three-dimensional (3D) counterparts are not frequently studied even though interesting magnetic properties should also be expected. In this regard, garnet with the general chemical formula $A_3B_2C_3O_{12}$ is an important material system in which the magnetic A cations form a 3D network of corner-sharing triangular lattices, named a hyper-Kagome lattice [24]. Among the rare-earth garnets, $Gd_3Ga_5O_{12}$ is the canonical frustrated magnet that shows a spin-liquid state down to 0.14 K [25], but developing a long-range hidden order [26]. In contrast, $Tb_3Ga_5O_{12}$ exhibits a long-range magnetic ordering below 0.35 K [27], while $Ho_3Ga_5O_{12}$ shows the coexistence of long- and short-range magnetic ordering below 0.6 K [28]. For these rare-earth gallium garnets, complex magnetic phase transitions can be induced by external magnetic fields. On the other hand, the transition-metal cations can also occupy the A site of naturally occurring aluminosilicate garnets, $A_3Al_2Si_3O_{12}$, e.g., spessartine for A = Mn and almandine for A = Fe [24]. For these cases, long-range antiferromagnetic (AF) ordering of Mn^{2+} or Fe^{2+} spins was found to take place at a higher temperature of $T_N \approx 7 - 8$ K [29–31]. The magnetic structure of $Mn_3Al_2Si_3O_{12}$ has been determined by neutron diffraction as a complex noncollinear triangular 12-sublattice AF ordering with the Mn^{2+} spins lying within the (111) plane and directed along the [–2 1 1] directions [29,32]. Still, the hyper-Kagome lattice has produced a moderate magnetic frustration in $Mn_3Al_2Si_3O_{12}$, for which the frustration index $f \equiv |\theta_{CW}/T_N|$ is about 3 given the Curie-Weiss temperature $\theta_{CW} = -20.8$ K and $T_N = 7$ K [30]. These results suggested that the geometrical frustration can be relieved substantially in these transition-metal aluminosilicate garnets due to the

*jgcheng@iphy.ac.cn

presence of 3D exchange interactions, but complex magnetic ordering can be realized in them.

Beyond the end members of naturally occurring $A_3Al_2Si_3O_{12}$ (A = Ca, Mg, Fe, Mn), there is a synthetic Co-garnet, $Co_3Al_2Si_3O_{12}$, which has been known since 1981 [33]. Depending on the synthesis conditions, $Co_3Al_2Si_3O_{12}$ can crystallize in two isostructural polymorphs, the α and β phase [33,34]. It was reported that the β phase prepared under 5 GPa and 900 °C can transform to the α polymorph upon compression to about 5 GPa at room temperature [35]. So far, the interest in $Co_3Al_2Si_3O_{12}$ resided mainly in the crystallographic features from the viewpoint of garnet crystal chemistry. But its magnetic properties, related to the magnetic Co^{2+} ions in the geometrically frustrated hyper-Kagome lattice, remain unknown to date.

The purpose of this paper is thus to unveil the magnetic properties of β-$Co_3Al_2Si_3O_{12}$, which was synthesized under high pressure and characterized by measurements of dc magnetic susceptibility, neutron powder diffraction, and specific heat. We find that β-$Co_3Al_2Si_3O_{12}$ undergoes a long-range AF transition at $T_N = 11$ K and forms a complex magnetic structure characterized by the coexistence of collinear and spiral magnetic ordering of Co^{2+} sublattices. We also observed a magnetic field induced spin-flop transition at $\mu_0 H_c \approx 4$T below T_N.

II. EXPERIMENTAL

Polycrystalline $Co_3Al_2Si_3O_{12}$ samples were prepared under high-pressure and high-temperature (HPHT) conditions using a Kawai-type multianvil module (Max Voggenreiter GmbH). The starting materials were high-purity CoO, Al_2O_3, and SiO_2 powders thoroughly mixed in the stoichiometric ratio. The precursor was contained in a Pt capsule, inserted into an h-BN (hexagonal Boron Nitride) sleeve, and then placed in a graphite furnace. The whole sample assembly was put in the central hole of a semisintered MgO ceramic octahedron that was used as the pressure transmitting medium. The pressure was first increased to 5.5 GPa, and then the temperature was raised to 1250 °C and kept for 2 h. The temperature was quenched to room temperature before releasing pressure slowly. The sample was recovered at ambient conditions and then subjected to various characterizations at ambient pressure.

The phase purity of the obtained product was first examined with powder x-ray diffraction (XRD) at room temperature. Low-temperature neutron powder-diffraction (NPD) data for $Co_3Al_2Si_3O_{12}$ were collected at the D20 high-flux diffractometer at Institut Laue Langevin, France, with $\lambda = 1.54$ Å and a takeoff angle of 90°, provided with a standard "orange" cryostat. About 2-g samples were contained in a vanadium sample holder of 6-mm diameter. A first diagram was collected at 200 K, counting for 1 h. After cooling down the sample to 2 K, a good-statistics pattern was acquired by counting at 2 K for 1 h. Then, a sequential acquisition was launched while warming at a rate of 0.30 Kmin^{-1}, with a counting time of 5 min per pattern. A final acquisition at 100 K for 1 h was carried out. The refinements of the crystal and magnetic structures were performed by the Rietveld method [36], using the FULLPROF refinement program

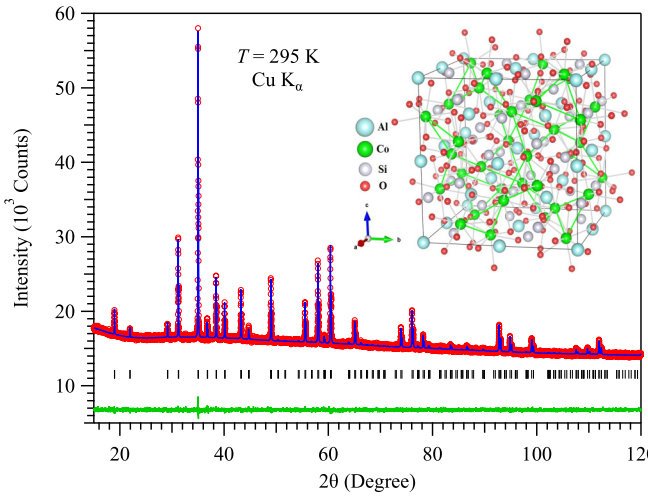

FIG. 1. Rietveld refinement plot based on the powder XRD pattern of $Co_3Al_2Si_3O_{12}$ at room temperature. Inset: Schematic view of the crystal structure.

[37]. A Thompson-Cox-Hastings pseudo-Voigt function with a phenomenological (fixed) correction for asymmetry due to the finite height of the 2D positional sensitive detector was used. The background was adjusted by a 24-terms Chebychev polynomial. The following parameters were refined in the final run: scale factor; background coefficients; three instrument corrections; zero-point error; the offsets proportional to $\cos(2\theta)$ and to $\sin(2\theta)$, responsible for the effective sample shifts perpendicular to and along the beam; profile parameters; atomic coordinates of oxygen, as the only atom with variable coordinates; the isotropic displacement parameters; as well as the Co magnetic moments in the magnetically ordered state. The bound neutron-scattering lengths and magnetic neutron-scattering form factors used were those internally tabulated in FULLPROF [37]. The magnetic properties were measured with a Quantum Design magnetic property measurement system (MPMS-III) up to 7 T and physical property measurement system (PPMS-14T) up to 14 T. The specific heat was measured with the two-tau relaxation method with a PPMS.

III. RESULTS AND DISCUSSIONS

In the previous report [34], β-$Co_3Al_2Si_3O_{12}$ garnet was synthesized at 5 GPa and 900 °C for 3 h. During the course of our HPHT experiments at 5.5 GPa, we found that the phase purity of the as-prepared sample depends sensitively on the reaction temperature. For the syntheses at 1100 °C and below, the reaction is incomplete as indicated by the presence of some unreacted Al_2O_3, SiO_2, and $CoSiO_3$ impurity in the final product, while the compound seems to be decomposed for the synthesis above 1400 °C. According to the XRD patterns, the reactions between 1200 and 1350 °C are completed and the major garnet phase can be harvested, but some minor impurity phases can still exist depending on the temperature, i.e., $CoAl_2O_4$ for 1200 °C and Co_2SiO_4 for 1350 °C. We finally obtained nearly pure $Co_3Al_2Si_3O_{12}$ garnet in a narrow temperature range around 1250 °C.

Figure 1 shows the XRD pattern of single-phase $Co_3Al_2Si_3O_{12}$ sample, which is purple in color in the powder

TABLE I. Crystal structural parameters of $Co_3Al_2Si_3O_{12}$ refined from powder x-ray diffraction (XRD) at 295 K and neutron diffraction (NPD) at 200 and 100 K in space group Ia-$3d$ (no. 230, $Z = 8$)[a]

T (K)	295	200	100
Method	XRD	NPD	NPD
a (Å)	11.45786(5)	11.4218(2)	11.4185(2)
V (Å^3)	1504.22(1)	1490.06(5)	1488.78(5)
x_O	0.0361(1)	0.03355(6)	0.03356(5)
y_O	0.0501(2)	0.05145(6)	0.05154(6)
z_O	0.6535(2)	0.65301(7)	0.65302(7)
R_p(%)	0.67	3.75	3.59
R_{Bragg}(%)	6.58	2.9	2.83

[a]Structural model: Co at 24c (1/8, 0, 1/4), Al at 16a (0, 0, 0), Si at 24d (3/8, 0, 1/4), O at 96h (x, y, z).

form. The crystal structure parameters were refined against the XRD data by the Rietveld method, using the standard cubic garnet structure model: space group Ia-$3d$ with Co in the 24c (1/8, 0, 1/4), Al in the 16a (0, 0, 0), Si in the 24d (3/8, 0, 1/4), and O in the 96h (x, y, z) sites, respectively [34]. As illustrated in Fig. 1, the refinement converged excellently. The obtained structural parameters are listed in Table I. The refined lattice parameter $a = 11.45786(5)$ Å is consistent with the previously reported value of 11.4603(2) Å for β-$Co_3Al_2Si_3O_{12}$ [34,38,39].

The refined crystal structure is depicted in the inset of Fig. 1. In the cubic garnet structure, the Co, Al, and Si atoms are coordinated by eight, six, and four oxygen atoms, forming a CoO_8 dodecahedron, AlO_6 octahedron, and SiO_4 tetrahedron, respectively. The Al-O and Si-O bonds in the corresponding polyhedra are all equal between each other. In the CoO_8 dodecahedron, two slightly different bond lengths exist; however, there is only one unique Co-O-Co angle relevant for the magnetic exchange, i.e., Co-O bonds: 2.351(2) Å and 2.227(2) Å, Co-O-Co = 100.03(6)° at 295 K. As mentioned above, one of the prominent features of the garnet structure is that the magnetic Co^{2+} ions form a 3D network of corner-sharing equilateral triangles. Specifically, each corner of every Co_3 triangle borders another Co_3 triangle, and the angle between the planes of these two Co_3 triangles is approximately 70.53°. As a geometrically frustrated lattice, it is interesting to investigate the magnetic properties of $Co_3Al_2Si_3O_{12}$ that have not been studied so far to our knowledge.

Figure 2(a) shows the temperature dependence of magnetic susceptibility $\chi(T)$ measured under an external magnetic field of $\mu_0 H = 1.0$T. The zero-field-cooled (ZFC) and field-cooled (FC) $\chi(T)$ curves are perfectly coinciding with each other, and the pronounced peak at $T_N = 11$K signals the onset of long-range AF order, which is further confirmed by NPD below. Fitting of $\chi^{-1}(T)$ to the Curie-Weiss law, i.e., $\chi(T) = C/(T - \theta_{CW})$, in the temperature range 150–300 K yields an effective magnetic moment $\mu_{eff} = (8C)^{1/2} = 4.98\mu_B/Co^{2+}$ and a Curie temperature $\theta_{CW} = -13.0$K. The obtained μ_{eff} is much larger than the expected spin-only value, $3.87\mu_B$, for high-spin Co^{2+} with spin 3/2. But it is in line with the typical values of $4.9 - 5.2\,\mu_B$ reported in literature for the compounds containing high-spin Co^{2+} ions such as the

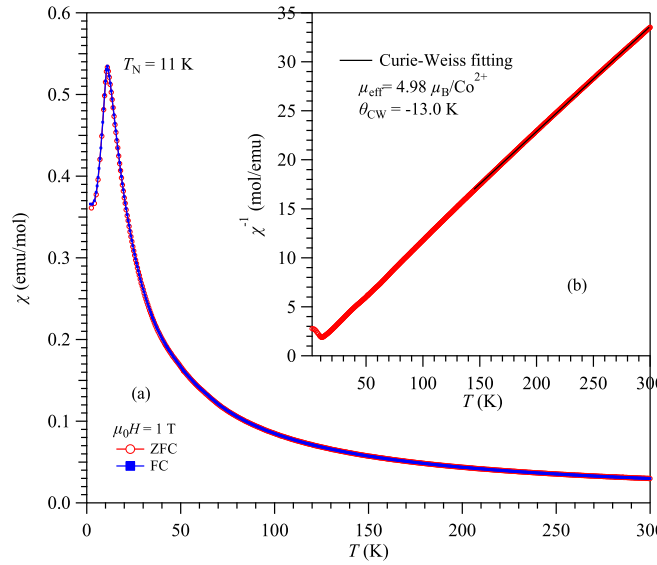

FIG. 2. (a) Temperature dependence of the dc magnetic susceptibility $\chi(T)$ for $Co_3Al_2Si_3O_{12}$ measured under 1 T in zero-field-cooled (ZFC) and field-cooled (FC) modes. (b) The Curie-Weiss fitting to the inverse susceptibility $\chi^{-1}(T)$ in the temperature range 150–300 K. The obtained effective magnetic moment μ_{eff} and Curie-Weiss temperature θ_{CW} are given in the figure; see the main text for details.

double perovskite Sr_2CoWO_6; see Ref. [40] and references therein. The observed large μ_{eff} has been attributed to the unquenched orbital magnetic contribution of the Co^{2+} ion [41]. The negative θ_{CW} suggests an overall AF exchange interaction in $Co_3Al_2Si_3O_{12}$. It is interesting to note that the magnetic frustration is almost absent, i.e., the frustration index $f \equiv |\theta_{CW}/T_N|$ is very close to unity, even though the Co^{2+} magnetic sublattice is featured by some geometrical frustration as mentioned above.

To understand how the magnetic frustration is relieved, we need to determine the magnetic structure of $Co_3Al_2Si_3O_{12}$. For this purpose, we prepared about 2-g samples from eight runs of HPHT syntheses under similar conditions. Each sample was carefully checked by XRD before mixing them together for the NPD measurements. Figure 3(a) displays a series of NPD patterns collected upon warming up from 2 to 25 K at a rate of 0.3 Kmin^{-1}. As can be clearly seen, some sharp diffraction peaks, e.g., at ~10.8°, 15.3°, and 33.1°, appear below ~12 K, signaling the occurrence of a long-range magnetic transition. This is in excellent agreement with the $\chi(T)$ results shown in Fig. 2. As illustrated in Fig. 3(a), some of the magnetic diffraction peaks are additional to those of the chemical cell diffraction peaks, while some coincide in position with those of the crystallographic cell. All magnetic diffraction peaks can be indexed with the propagation vector of magnetic ordering $k = (0, 0, 0)$, and the symmetry analysis of possible magnetic ordering schemes for magnetic Co atoms located at the 24c (1/8, 0, 1/4) sites was carried out with the Isotropy Software Suite [42], the online tools of the Bilbao Crystallographic server, based on the considerations of magnetic symmetry explained in Ref. [43]. The following maximal magnetic space groups of Ia-$3d$ can provide possibilities for the Co atom to order magnetically with a propagation

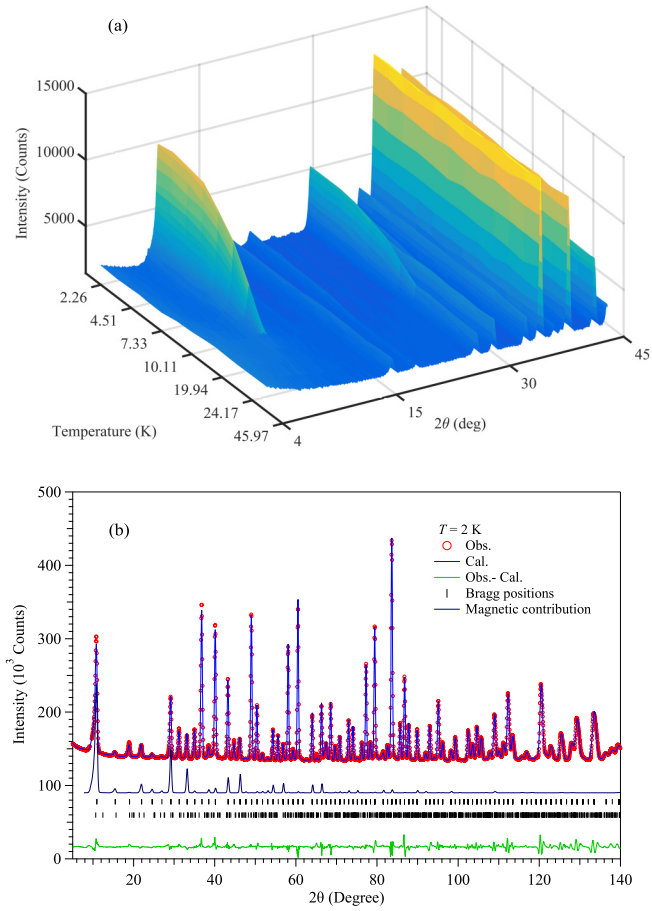

FIG. 3. (a) A series of NPD patterns collected upon warming up from 2 to 25 K. (b) Refinement based on the NPD pattern at 2 K. A solid line below the graph shows the calculated contribution of the magnetic diffraction to the total calculated intensity, and the two rows of ticks indicate the calculated peak positions of the chemical and magnetic diffraction.

vector $k = (0, 0, 0)$, viz., Ia-$3d'$ (no. 230.148), Ia'-$3'd$ (no. 230.147), $I4'_1/a'cd'$ (no. 142.568), $I4_1/ac'd'$ (no. 142.567), $I4'_1/ac'd$ (no. 142.564), $I4_1/a'cd$ (no. 142.563), $Fd'd'd$ (no. 70.530), and $Fd'dd$ (no. 70.529).

All possibilities were carefully checked in the refinements. For two of them, $I4'_1/a'cd'$ (no. 142.568) and $I4'_1/ac'd$ (no. 142.564), the Co site splits into two, whereby one of them would have zero moment, and these are proved to be incorrect as being checked versus the experimental data. We finally found the solution just in one of the possible magnetic space groups, namely, in the magnetic space group $I4_1/a'cd$ (no. 142.563). Co site thereby splits into two: Co1 (1/8,0,1/4) and Co2 (1/4,1/8,0), the former allowing for only one moment component M_x, and the latter allowing for M_x and M_z. Keeping in mind that the crystal structure is preserved to be cubic and there is in reality only one type of Co atoms in the structure, we have constrained the amplitude of the moments on both Co sites to be identical. This assumption proves to provide a working magnetic structure model allowing for sufficiently good refinement, so any deviations from this first–guess approach of the equal moment magnitudes–would appear to be not statistically justified, for it cannot be verified within the available data quality. Further constraints were employed as well in order to preserve ideally undistorted cubic structure, i.e. the general 96h (x, y, z) site of oxygen in the Ia-$3d$ space group splits into three general 32-fold (x, y, z) sites in the $I4_1/a'cd$ space group, and these were constrained to be cyclically equal: $(x, y, z)_{O1} = (y, z, x)_{O2} = (z, x, y)_{O3}$. Additionally, the lattice constants were constrained to be equal to preserve the cubic symmetry. Figure 3(b) displays the refinement plot for NPD at 2 K, in which the dark blue line is the contribution of the magnetic diffraction of ordered Co moments to the total diffraction pattern. The structural parameters at 2 K after refinement are listed in Table II. The Co moment is refined to be $\sim 3.45(2)\mu_B$ at 2 K.

While being on average antiferromagnetic, $Co_3Al_2Si_3O_{12}$ actually adopts quite a complex magnetic structure as illustrated in Fig. 4 viewed along different crystallographic axes. As can be seen in Fig. 4(a), a simple collinear AF order is realized along the a-axis direction for the sublattice of Co1 shown in red. In contrast, the sublattice of Co2 atoms (in green) carrying moments inclined to the a axis at $\sim 35.3°$ is more complex. The Co2 atoms form spirals with cyclically varying magnetic moments and propagating along the direction parallel to the a axis; the nearest-neighbor (NN) spins in each spiral have the same angle of $\sim 48.23°$. As illustrated in Fig. 4(d), these spirals form a square lattice, commensurate with the chemical cell, and each neighboring spiral along either b or c exhibits the opposite direction of moments. Therefore, the complex AF structure of $Co_3Al_2Si_3O_{12}$ is characterized by the coexistence of collinear and spiral magnetic ordering of Co^{2+} moments.

To have a better understanding of the complex magnetic structure, here we describe in detail how the collinearly aligned Co1 and spirally arranged Co2 spins are connected with each other to form the corner-sharing Co_3 triangles. As mentioned above, the neighboring Co_3 triangles are twisted with each other, forming an angle of $\sim 70.53°$ between the planes of two connected triangles. A closer inspection of the magnetic structure in Fig. 4(a) actually reveals two types of Co_3-triangle pairs, which share a common Co1 or Co2 atom, respectively.

For the triangle pairs sharing a common Co1 atom, Fig. 4(b), the spin of Co1 has the same angle of $\sim 35.3°$ with respect to all the other Co2 moments at the countersides of the two bordering triangles. These Co2 atoms are belonging to the spirals that are running with offset of (0,1/2,1/2) within a unit cell. It is noteworthy that the Co1-Co2 angle of 35.3° is exactly half of the "twisting" angle between these two triangles. The Co2 moments pointing outward of the triangles are almost ideally lying in the corresponding triangles planes and make an angle of 48.23° with respect to the other Co2 moment in the same triangle. Thus, all the nearest-neighbor Co-Co couplings are rather close to ferromagnetic (FM), which is consistent with the general superexchange considerations as discussed below.

For the triangle pairs sharing a common Co2 atom, Fig. 4(c), the moments of the central Co2 atoms are lying almost ideally along the bisecting line of both triangles. In both neighboring triangles, it is again rather ferromagnetically coupled to the other two Co2 spins, forming the individual

TABLE II. Crystal structural parameters of $Co_3Al_2Si_3O_{12}$ refined from neutron powder-diffraction data at 2 K[a] for magnetic space group $I4_1/a'cd$(no.142.563 in BNS notations, $Z = 8$) with the lattice parameters $a = 11.4147(3)$ Å and $V = 1487.30(7)$Å^3.

Atom	Multiplicity	X	y	z	Occ.
Co1	8	1/8	0	1/4	0.25
Co2	16	1/4	1/8	0	0.5
Al	16	0	0	0	0.5
Si1	8	3/8	0	1/4	0.25
Si2	16	1/4	3/8	0	0.5
O1	32	0.03357(6)	0.05166(6)	0.65303(7)	1
O2	32	0.65303(7)	0.03357(6)	0.05166(6)	1
O3	32	0.05166(6)	0.65303(7)	0.03357(6)	1

[a]Reliability factors: $R_p(\%) = 3.71$, $R_{Bragg}(\%) = 2.83$.

spirals, and to the two Co1 moments, which bridge with other spirals. Again, the angle of the Co2-Co2 moments is 48.23°, and that of Co2-Co1 moments is 35.3°. These junctions with Co2 in the middle of two triangles are linking the Co1 moments along both b and c directions. There are exactly twice as many of these triangle pairs as of those with Co1 in the middle.

Based on the above detailed descriptions, we can see a very interesting situation here in $Co_3Al_2Si_3O_{12}$; i.e., although all NN Co-Co pairs have an effectively ferromagnetic, though slightly canted, interaction, we finally have an overall long-range antiferromagnetically ordered commensurate structure. As will be discussed below, it should be the further-neighbor (FN) AF couplings that lead to the complex magnetic structure.

Figure 5 summarizes the temperature dependences of crystal and magnetic structural parameters. As shown in Fig. 5(a), the lattice parameter a decreases smoothly upon cooling and tends to level off below 40 K. Except for a few spurious points around 20 K with unknown origin, no clear anomalies are observed around T_N, signaling the absence of significant magnetoelastic coupling in this compound. The internal structure details show no clear changes as the sample enters the magnetically ordered state. As shown in Fig. 5(b), the two different Co-O distances do not show any effect at T_N, and the single Co-O-Co bond angle does not have any peculiarities either. The Co moment increases gradually upon cooling across T_N, Fig. 5(c), but the angle between moments of Co1 (i.e., a axis) and Co2 seems to be almost constant at ∼35° below T_N, Fig. 5(d). The magnetic contribution to the pattern

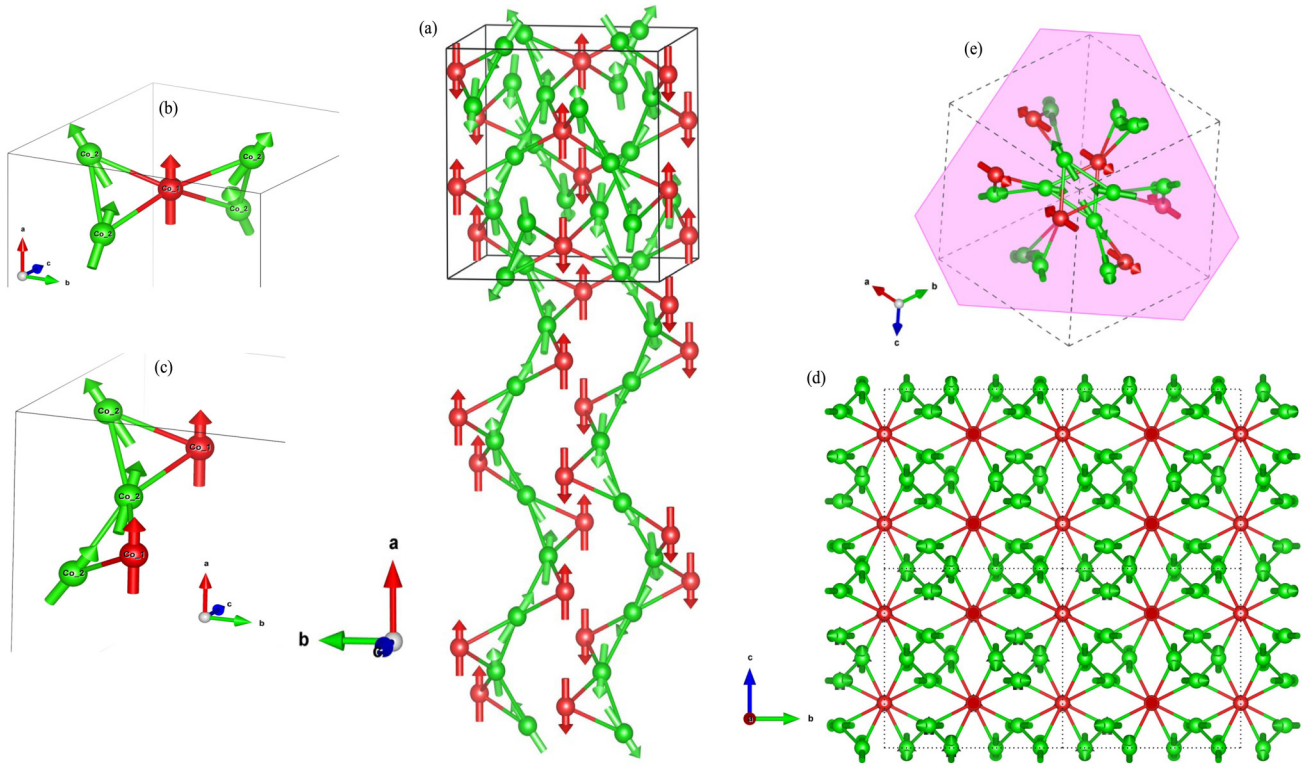

FIG. 4. (a, d, e) Schematic views of the magnetic structure of $Co_3Al_2Si_3O_{12}$ along different crystallographic axes. (b, c) Two types of Co_3-triangle pairs sharing a common Co1 or Co2 atom, respectively.

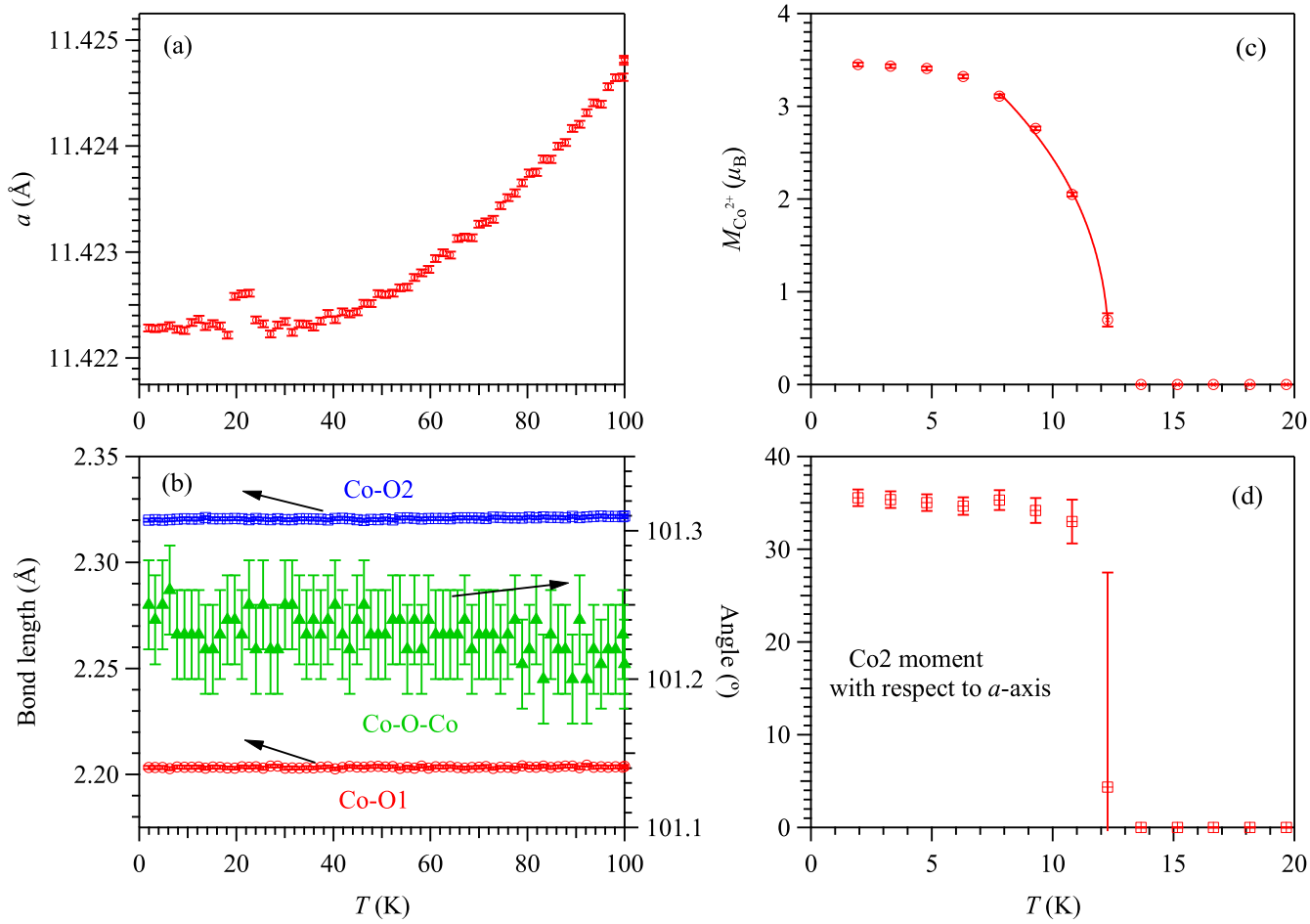

FIG. 5. Temperature dependences of (a) lattice parameter a, (b) the Co-O bond lengths and the Co-O-Co bond angle, (c) the Co magnetic moment, and (d) the angle between the Co2 moment and the crystallographic a axis.

at ∼12 K was already rather weak, which did not allow us to safely determine the exact orientation of the Co magnetic moments just below T_N. It looks, though, as if a tendency might exist for this angle to decrease when approaching the T_N.

To study the effect of external magnetic field on the noncollinear spin structure, we also measured the magnetization and magnetic susceptibility under different fields. Figure 6(a) shows the field dependence of magnetization $M(H)$ of $Co_3Al_2Si_3O_{12}$ measured at 2 K and up to 14 T. As can be seen, $M(H)$ approaches a saturation moment of $M_s \sim 3.0\mu_B/Co^{2+}$, which is in line with the high-spin Co^{2+} ion with spin 3/2. In addition, there is an obvious slope change (or fast increase) of $M(H)$ at about $H_c \sim 4.0$ T where the magnetization corresponds to $\sim 1/3M_s$. Figure 6(b) shows the $M(H)$ curves at different temperatures. This anomaly becomes weaker and shifts to lower magnetic fields with increasing temperature, and eventually smears out at $T \geqslant T_N$. The observed slope change of $M(H)$ at H_c suggests a possible spin-flop transition induced by an external magnetic field. In Fig. 6(b), we used the derivative of $M(H)$ to define the critical field H_c for this transition. The temperature dependence of H_c is shown in Fig. 6(d), which illustrates a gradual reduction of H_c upon approaching T_N. The field induced change is also reflected in the $\chi(T)$ curves around T_N shown in Fig. 6(c). For $H < H_c$, $\chi(T)$ exhibits a pronounced peak at T_N, which shifts to lower temperatures with increasing the field. However, under fields higher than H_c, such as 5 and 7 T, $\chi(T)$ shows no sharp peak but exhibits more like a flat regime below the transition temperature. This change again indicates a possible transition to a canted AF or partially spin-polarized state above H_c. Based on the $M(H)$ and $\chi(T)$ data, we propose an H-T magnetic phase diagram of $Co_3Al_2Si_3O_{12}$ as shown in Fig. 6(d).

The presence of long-range AF order and the influence of external magnetic fields is also studied by the specific-heat $C(T)$ measurements. The main panel of Fig. 7 displays the measured total $C(T)$ of $Co_3Al_2Si_3O_{12}$ at zero field, in which the long-range AF order produces a pronounced anomaly peaked at $T_N = 10.2$ K. Since $Co_3Al_2Si_3O_{12}$ is an AF insulator, its $C(T)$ mainly consists of lattice, C_{lat}, and magnetic, C_m, contributions. Considering the fact that C_m occurs mainly in the vicinity of T_N, we have attributed the total $C(T)$ in the temperature range 40–250 K to C_{lat}, and simulated it by considering three Einstein modes, viz.,

$$C(T) = \sum_{i=1}^{3} f_{Ei} \times 3nR\left(\frac{\theta_{Ei}}{T}\right)^2 \frac{\exp\left(\frac{\theta_{Ei}}{T}\right)}{\left[\exp\left(\frac{\theta_{Ei}}{T}\right) - 1\right]^2} \qquad (1)$$

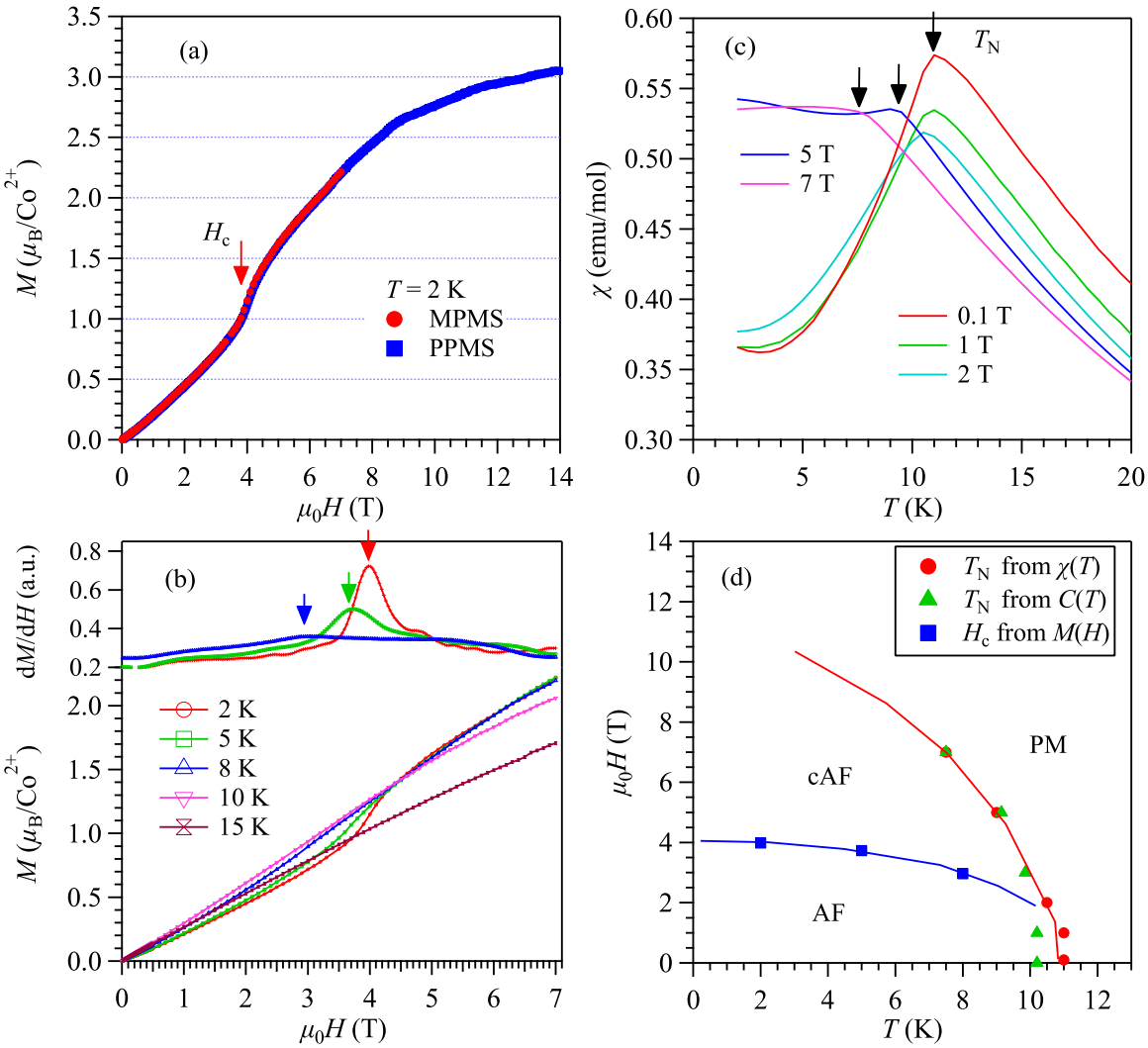

FIG. 6. (a) Field dependence of the magnetization $M(H)$ at 2 K measured with MPMS up to 7 T and with PPMS up to 14 T. (b) Isothermal magnetization $M(H)$ curves and their field derivative curves at various temperatures up to 15 K. (c) Temperature dependence of magnetic susceptibility $\chi(T)$ under different external magnetic fields up to 7 T. (d) Field-temperature phase diagram of $Co_3Al_2Si_3O_{12}$. AF, cAF, and PM stand for antiferromagnetic, canted antiferromagnetic, and paramagnetic, respectively.

where θ_{Ei} and f_{Ei} are the Einstein temperature and the corresponding fraction for each mode, $n = 20$ is the number of atoms in the formula unit, and $R = 8.314\,\mathrm{J/mol\,K}$ is the ideal gas constant. As illustrated by the solid line in Fig. 7(a), the $C(T)$ between 40 and 250 K can be described excellently by C_{lat} and the obtained parameters are $\theta_{E1} = 143(16)\,\mathrm{K}$, $f_{E1} = 0.13(3)$; $\theta_{E2} = 394(34)\,\mathrm{K}$, $f_{E2} = 0.36(2)$; and $\theta_{E3} = 928(55)\,\mathrm{K}$, $f_{E3} = 0.50(2)$. Then, $C_m(T)$ is obtained by subtracting C_{lat} from the total $C(T)$.

Figure 7(b) displays the temperaure dependence of $C_m(T)$ and the magnetic entropy $S(T)$ associated with the Co^{2+} spins below 40 K. The resultant S value of $\sim 30\,\mathrm{J/mol\,K}$ accounts for ~87% of the expected magnetic entropy $S_{exp} = 34.57\,\mathrm{J/mol\,K}$ for the Co^{2+} ions with spin 3/2. The slight discrepancy should arise from the overestimation of C_{lat} in the above analysis. Alternatively, a more careful comparison with the specific heat of an isostructural, nonmagnetic analog compound, such as $Ca_3Al_2Si_3O_{12}$, might be helpful to resolve this issue.

We also measured the $C(T)$ of $Co_3Al_2Si_3O_{12}$ below 40 K under various magnetic fields up to 7 T. Figure 7(c) displays the magnetic contribution $C_m(T)$ at different fields by subtracting the $C_{lat}(T)$ at zero field. As can be seen, both the transition temperature and the magnitude of the specific-heat peak at T_N decrease gradually with increasing magnetic field. In addition, a broad hump appears at $T > T_N$ in $C(T)$ under 7 T due to the development of a partially spin-polarized state. As shown in Fig. 6(a), the $M(H)$ curve at 2 K first increases linearly as it should do in an antiferromagnet, then above the spin-flop transition at $H_c \approx 4\,\mathrm{T}$ it varies like in a ferromagnet while approaching the saturation value for a parallel alignment of spins, or a fully polarized state. Thus, under a high magnetic field of $7\,\mathrm{T} > H_c$, the system lies in the partially polarized state, and the spins even in the paramagnetic state are partially aligned with strong short-range correlations. Then, the magnetic entropy is relieved gradually from a temperature higher than the long-range ordering temperature, resulting in a broad hump above T_N. These results are in line with

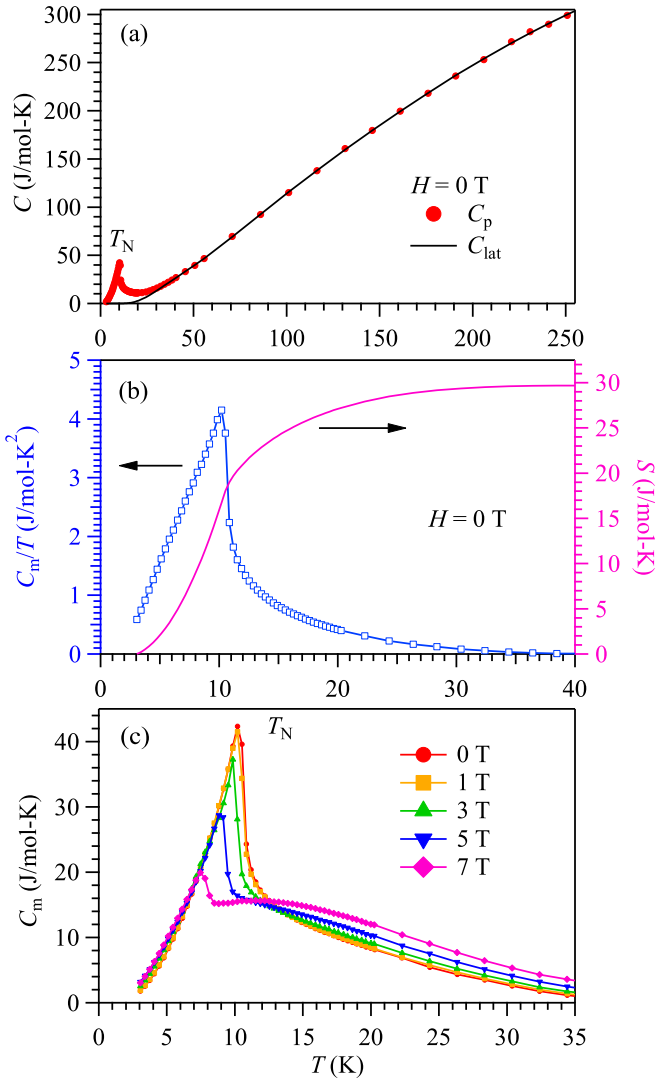

FIG. 7. (a) Temperature dependence of specific heat $C(T)$ of $Co_3Al_2Si_3O_{12}$ in the wide temperature range from 2 to 250 K under zero field. The solid line represents the lattice contribution C_{lat} as detailed in the main text. (b) The magnetic contribution C_m and the corresponding entropy S at zero field. (c) Temperature dependence of $C_m(T)$ under various magnetic fields.

the $\chi(T)$ data shown in Fig. 6(c). The value of T_N obtained from $C(T)$ is also given in Fig. 6(d), which delineates the phase boundary between the magnetically ordered and the paramagnetic phases.

Based on the above characterizations, we have established that the synthetic garnet $Co_3Al_2Si_3O_{12}$ enters a long-range AF ordered state below $T_N \approx 11$ K with a complex spin structure, which then experiences a magnetic field induced spin-flop transition at $H_c \approx 4$ T. First, it is instructive to compare the magnetic structure of $Co_3Al_2Si_3O_{12}$ with that of isostructural $Mn_3Al_2Si_3O_{12}$, in which all the Mn^{2+} spins lie in the (111) plane and form a 120° triangular AF arrangement [29,35]. As seen in Fig. 4(e), the magnetic structure of $Co_3Al_2Si_3O_{12}$ viewed along the [111] direction is distinct from that of $Mn_3Al_2Si_3O_{12}$ [29]. In the present case, the Co^{2+} spins in $Co_3Al_2Si_3O_{12}$ are not confined within the (111) plane. Second, the stabilization of such a complex noncollinear and noncoplanar spin structure in $Co_3Al_2Si_3O_{12}$ indicates the presence of competing AF and FM superexchange interactions among the Co^{2+} spins. In the garnet structure, each Co dodecahedron is surrounded by two edge-sharing and four corner-sharing Si tetrahedra, four edge-sharing Al octahedra, and four edge-sharing Co dodecahedra. The NN Co-O-Co superexchange interaction with an angle ~100°, which is close to 90°, is expected to be FM. Indeed, the local spin arrangements within each triangle are close to FM, though slightly tilted, as shown in Figs. 4(b) and 4(c). This can also explain the absence of magnetic frustration in this system. On the other hand, the magnetic coupling between distant Co^{2+} spins via Al octahedra and Si tetrahedra should be weakly AF. Although the individual FN AF interaction should be weaker than that of NN FM interaction, the number of FN AF pathways is much higher than that of the NN FM pathways. As such, the system ends up with a complex noncollinear AF spin structure and manifests an overall AF exchange interaction as reflected by the negative $\theta_{CW} = -13$ K. Detailed calculations on these magnetic interactions over different pathways are needed in order to further understand the complex AF structure in $Co_3Al_2Si_3O_{12}$.

Finally, we note that the observation of spin-flop transition in $M(H)$ below T_N is manifested as a kinklike anomaly at $1/3M_s$, rather than a plateau over a finite field range as observed in many q2D TLAFs. Theoretically, it was predicted that a $1/3M_s$ plateau corresponding to a collinear uud state can occur over a finite field range in the 3D garnet antiferromagnet with spin-1/2 [44]. But the width of the plateau may shrink quickly with increasing the spin number. Whether the $1/3M_s$ plateau becomes diminished in this spin-3/2 system or can be visible at much lower temperatures deserves further studies on high-quality single-crystal samples.

IV. CONCLUSION

In summary, we have synthesized the cubic garnet $Co_3Al_2Si_3O_{12}$ under high-pressure and high-temperature conditions and investigated its magnetic properties via measurements of dc magnetic susceptibility, neutron powder diffraction, and specific heat as a function of temperature and/or external field. We found that $Co_3Al_2Si_3O_{12}$ undergoes a transition at $T_N = 11$ K to an antiferromagnetically ordered state with a complex spin structure, which is characterized by two distinct Co sublattices forming a collinear antiferromagnetic and a commensurate spiral magnetic ordering pattern, respectively. Interestingly, the determined magnetic structure is not frustrated as a result of dominant nearest-neighbor ferromagnetic interactions. It is the competition with the further-neighbor antiferromagnetic couplings that leads to a very special spin order. In addition, field induced spin-flop transition at $H_c \sim 4$ T was also observed below T_N.

ACKNOWLEDGMENTS

Work at IOPCAS is supported by the National Key Research and Development Program of China (Grant No. 2018YFA0305700), the National Natural Science Foundation of China (Grants No. 11921004, No. 11834016, and No.

11874400), the Beijing Natural Science Foundation (Grant No. Z190008), the Strategic Priority Research Program and Key Research Program of Frontier Sciences of the Chinese Academy of Sciences (CAS, Grants No. XDB25000000 and No. QYZDB-SSW-SLH013), and the CAS Interdisciplinary Innovation Team (Grant No. JCTD-2019-001). J.A.A. gratefully acknowledges the Spanish MINECO for granting Project No. MAT2017-84496-R. Q.H. and H.D.Z. acknowledge support from NSF-DMR through Grant No. DMR-1350002. The research at HFIR/ORNL was sponsored by the Scientific User Facilities Division, Office of Basic Energy Sciences, US Department of Energy. We are grateful to the Institut Laue-Langevin for making neutron beam time available.

[1] J. E. Greedan, J. Mater. Chem. **11**, 37 (2001).
[2] Y. Li, G. Chen, W. Tong, L. Pi, J. Liu, Z. Yang, X. Wang, and Q. Zhang, Phys. Rev. Lett. **115**, 167203 (2015).
[3] Y. Li, H. Liao, Z. Zhang, S. Li, F. Jin, L. Ling, L. Zhang, Y. Zou, L. Pi, Z. Yang, J. Wang, Z. Wu, and Q. Zhang, Sci. Rep. **5**, 16419 (2015).
[4] J. A. M. Paddison, M. Daum, Z. Dun, G. Ehlers, Y. Liu, M. B. Stone, H. Zhou, and M. Mourigal, Nat. Phys. **13**, 117 (2016).
[5] J. Sichelschmidt, P. Schlender, B. Schmidt, M. Baenitz, and T. Doert, J. Phys. Condens. Matter. **31**, 205601 (2019).
[6] J. G. Cheng, G. Li, L. Balicas, J. S. Zhou, J. B. Goodenough, C. Xu, and H. D. Zhou, Phys. Rev. Lett. **107**, 197204 (2011).
[7] J. A. Quilliam, F. Bert, A. Manseau, C. Darie, C. Guillot-Deudon, C. Payen, C. Baines, A. Amato, and P. Mendels, Phys. Rev. B **93**, 214432 (2016).
[8] T. Imai, E. A. Nytko, B. M. Bartlett, M. P. Shores, and D. G. Nocera, Phys. Rev. Lett. **100**, 077203 (2008).
[9] A. Zorko, S. Nellutla, J. van Tol, L. C. Brunel, F. Bert, F. Duc, J. C. Trombe, M. A. de Vries, A. Harrison, and P. Mendels, Phys. Rev. Lett. **101**, 026405 (2008).
[10] J. Alicea, A. V. Chubukov, and O. A. Starykh, Phys. Rev. Lett. **102**, 137201 (2009).
[11] A. V. Chubukov and D. I. Golosov, J. Phys. Condens. Matter. **3**, 69 (1991).
[12] S. Miyahara, K. Ogino, and N. Furukawa, Physica B: Condensed Matter **378–380**, 587 (2006).
[13] N. A. Fortune, S. T. Hannahs, Y. Yoshida, T. E. Sherline, T. Ono, H. Tanaka, and Y. Takano, Phys. Rev. Lett. **102**, 257201 (2009).
[14] T. Ono, H. Tanaka, H. Aruga Katori, F. Ishikawa, H. Mitamura, and T. Goto, Phys. Rev. B **67**, 104431 (2003).
[15] Y. Shirata, H. Tanaka, A. Matsuo, and K. Kindo, Phys. Rev. Lett. **108**, 057205 (2012).
[16] T. Susuki, N. Kurita, T. Tanaka, H. Nojiri, A. Matsuo, K. Kindo, and H. Tanaka, Phys. Rev. Lett. **110**, 267201 (2013).
[17] H. D. Zhou, C. Xu, A. M. Hallas, H. J. Silverstein, C. R. Wiebe, I. Umegaki, J. Q. Yan, T. P. Murphy, J.-H. Park, Y. Qiu, J. R. D. Copley, J. S. Gardner, and Y. Takano, Phys. Rev. Lett. **109**, 267206 (2012).
[18] J. Hwang, E. S. Choi, F. Ye, C. R. Dela Cruz, Y. Xin, H. D. Zhou, and P. Schlottmann, Phys. Rev. Lett. **109**, 257205 (2012).
[19] Y. Shirata, H. Tanaka, T. Ono, A. Matsuo, K. Kindo, and H. Nakano, J. Phys. Soc. Jpn. **80**, 093702 (2011).
[20] A. I. Smirnov, H. Yashiro, S. Kimura, M. Hagiwara, Y. Narumi, K. Kindo, A. Kikkawa, K. Katsumata, A. Y. Shapiro, and L. N. Demianets, Phys. Rev. B **75**, 134412 (2007).
[21] L. E. Svistov, A. I. Smirnov, L. A. Prozorova, O. A. Petrenko, L. N. Demianets, and A. Y. Shapiro, Phys. Rev. B **67**, 094434 (2003).
[22] Y. Doi, Y. Hinatsu, and K. Ohoyama, J. Phys. Condens. Matter. **16**, 8923 (2004).
[23] R. Ishii, S. Tanaka, K. Onuma, Y. Nambu, M. Tokunaga, T. Sakakibara, N. Kawashima, Y. Maeno, C. Broholm, D. P. Gautreaux, J. Y. Chan, and S. Nakatsuji, Europhys. Lett. **94**, 17001 (2011).
[24] K. P. Belov and V. I. Sokolv, Sov. Phys. Usp. **20**, 149 (1977).
[25] P. Schiffer, A. P. Ramirez, D. A. Huse, P. L. Gammel, U. Yaron, D. J. Bishop, and A. J. Valentino, Phys. Rev. Lett. **74**, 2379 (1995).
[26] J. A. M. Paddison, H. Jacobsen, O. A. Petrenko, M. T. Fernandez-Diaz, P. P. Deen, and A. L. Goodwin, Science **350**, 179 (2015).
[27] K. Kamazawa, D. Louca, R. Morinaga, T. J. Sato, Q. Huang, J. R. D. Copley, and Y. Qiu, Phys. Rev. B **78**, 064412 (2008).
[28] H. D. Zhou, C. R. Wiebe, L. Balicas, Y. J. Yo, Y. Qiu, J. R. D. Copley, and J. S. Gardner, Phys. Rev. B **78**, 140406(R) (2008).
[29] W. Prandl, Phys. Status Solidi B **55**, K159 (1973).
[30] G. C. Lau, T. Klimczuk, F. Ronning, T. M. McQueen, and R. J. Cava, Phys. Rev. B **80**, 214414 (2009).
[31] J. C. P. de Oliveria, M. de Costa, W. Schreiner, and A. Vasquez, J. Mag. Mag. Mater. **79**, 1 (1989).
[32] R. Plumier, Solid State Comm. **12**, 109 (1973).
[33] H. Ohashi, T. Fujita, and T. Osawa, J. Jpn. Assoc. Mineral. Petrol. Econ. Geol. **76**, 58 (1981).
[34] H. Ohashi, T. Osawa, and A. Sato, Acta Crystallogr. **C51**, 2213 (1995).
[35] M. N. Taran, F. Nestola, H. Ohashi, M. Koch-Muller, T. Balic-Zunic, and L. A. Olsen, Am. Miner. **92**, 1616 (2007).
[36] H. M. Rietveld, J. Appl. Crystallogr. **2**, 65 (1969).
[37] J. Rodriguez-Carvajal, Physica B **192**, 55 (1993).
[38] L. Dubrovinsky, N. Dubrovinskaia, I. Kantor, F. Nestola, and D. Gatta, High Pressure Res. **26**, 137 (2006).
[39] M. Tribaudino and H. Ohashi, Period. Mineral. **80**, 135 (2011).
[40] M. C. Viola, M. J. Martinez-Lope, J. A. Alonso, J. L. Martinez, J. M. De Paoli, S. Pagola, J. C. Pedregosa, M. T. Fernandez-Diaz, and R. E. Carbonio, Chem. Mater. **15**, 1655 (2003).
[41] C. A. Lopez, M. E. Saleta, J. Curiale, and R. D. Sanchez, Mater. Res. Bull. **47**, 1158 (2012).
[42] H. T. Stokes, D. M. Hatch, and B. J. Campbell, ISOTROPY Software Suite, iso.byu.edu.
[43] J. M. Perez-Mato, S. V. Gallego, E. S. Tasci, L. Elcoro, G. de la Flor, and M. I. Aroyo, Annu. Rev. Mater. Res. **45**, 217 (2015).
[44] M. E. Zhitomirsky, A. Honecker, and O. A. Petrenko, Phys. Rev. Lett. **85**, 3269 (2000).